Electronic Supplementary Information

CoFe formic-acid framework derived S, N co-doped carbon nanotube composites decorated with bimetallic sulfide as bifunctional electrocatalyst for rechargeable zinc-air batteries

Qihao Wu,‡[a] Tao Xie,‡[a] Li Zhang,*[a, b] Heju Gao,[a] Jiahui Jiang,[a] Ting Zhao,[a] Guancheng Xu*[a]

[a] State Key Laboratory of Chemistry and Utilization of Carbon Based Energy Resources; College of Chemistry, Xinjiang University, Urumqi, 830046, Xinjiang, PR China.

[b] College of Chemical Engineering, Xinjiang University, Urumqi, 830046, Xinjiang, PR China.

‡ These authors contributed equally to this work.

* Corresponding author.

E-mail: zhangli420@xju.edu.cn, xuguanchengxju@163.com

1 Materials characterization

The crystalline phase structure of samples were characterized by powder X-ray diffraction (XRD, Bruker D8 advance diffractometer, Cu Kα radiation, λ = 0.15405 nm). And the morphological images of samples were acquired by scanning electron microscopy (SEM, Hitachi S-4800). The morphology and microstructure of the sample was characterised using transmission electron microscopy (TEM, JEOL Ltd. JEM F200). The elemental content and distribution of the compounds were analyzed by X-ray energy dispersive spectroscopy (EDS) and elemental mapping (FE-SEM, Hitachi SU8010 microscope). The contents of ingredients were detected by X-ray photoelectron spectroscopy (XPS, Escalab 250 Xi, Thermo Fisher Scientific). The degree of graphitization of carbon matrix in the samples was characterized by Raman spectroscopy (Raman, Bruker Senterra R 200-L). The elemental composition of the sample was performed using Elementary Analyzer (EA, Elementar Elementar Vario EL cube). The elemental composition of the sample was performed using inductively coupled plasma (ICP, Thermo ESCALAB 250 Xi).

2 Electrochemical measurement

All electrochemical tests were all performed at room temperature in a standard three-electrode system using a CHI 760E electrochemical workstation. The Ag/AgCl or Hg/HgO electrode and graphite rod were used as the reference and counter electrode, respectively. All measured potential were converted to the reversible hydrogen electrode (RHE) scale according to the Nernst equation ($E_{RHE} = E_{Ag/AgCl\ or\ Hg/HgO} + 0.059pH + E^{\theta}$).

2.1 Working electrode preparation

The working electrode was prepared as follows: 2.5 mg of the catalyst was firstly dispersed in a mixed solution (500 μL) of water/ethanol/Nafion with a volume ratio of 12:12:1, and then sonicated for 1 h to form a uniform catalyst ink. Afterwards, 10 μL of catalyst ink was loaded onto a glassy carbon electrode with a diameter of 5.0 mm. After drying at room temperature for 0.5 h, a working electrode was obtained.

2.2 Electrochemical test method of ORR

The electrocatalytic ORR performance evaluation was performed in a standard three-electrode cell. The electrochemical performance was tested using graphite rods as counter electrode, drop-coated catalyst GCE as working electrode, and Ag/AgCl as reference electrode using electrochemical workstation CHI 760E. Cyclic voltammetry (CV) measurements were performed in N_2 or O_2-saturated 0.1 M KOH solutions with a potential range from 0 to 1.2 V at a scan rate of 50 mV s^{-1}. Linear sweep voltammetry (LSV) curves were recorded during the 1600 rpm rotating disk electrode test. The stability of the catalysts was assessed by chronoamperometry for 1600 rpm at 0.2 V.

The electron transfer number (n) was further obtained from LSV curves measured at various rotating speeds (400-2025 rpm), and calculated according to Equation (1) and (2).

$$\frac{1}{j} = \frac{1}{j_L} + \frac{1}{j_K} = \frac{1}{B\omega^{1/2}} + \frac{1}{j_K} \quad (1)$$

$$B = 0.2nFC_o(D_o)^{2/3}\nu^{-1/6} \quad (2)$$

And the kinetic current density (j_K) was also calculated from equation (3).

$$j_K = \frac{j_L \times j}{j_L - j} \quad (3)$$

Where j and j_L is the measured and diffusion-limited current densities (mA cm^{-2}), respectively. ω is the electrode rotating speed (rpm). B is the reciprocal of the slope determined from the Koutecky-Levitch (K-L) plots, and n is the number of electrons transferred per oxygen molecule. F is the Faraday constant (96485 C mol^{-1}); C_o is the concentration of O_2 (1.2×10^{-6} mol cm^{-3}) in solution; v is the kinetic viscosity (0.01 cm^2 s^{-1}), and D_o is the diffusion coefficient of O_2 in 0.1 M KOH (1.9×10^{-5} cm^2 s^{-1}).

The n and H_2O_2 yield for catalysts were examined by rotating ring-disk electrode techniques and calculated according to equation (4) and (5).

$$H_2O_2(\%) = 200 \times \frac{I_R/N}{I_D + I_R/N} \quad (4)$$

$$n = 4 \times \frac{I_D}{I_D + I_R/N} \quad (5)$$

Here, I_D and I_R are the disk and ring currents, respectively, and N ($\sim$0.47) is the current collection efficiency of the Pt ring.

2.3 Electrochemical test method of OER

The electrocatalytic OER performance evaluation was performed in a standard three-electrode cell. The electrochemical performance was tested using graphite rods as counter electrode, drop-coated catalyst GCE as working electrode, and Hg/HgO as reference electrode using electrochemical workstation CHI 760E. LSV curves were obtained in 1 M KOH solution at a scan rate of 5 mV s^{-1} over a voltage range of 1.0 to 1.8 V.

The electrochemical AC impedance spectra (EIS) were obtained using an AC current of 5 mV in the frequency range of 100000 to 0.1 Hz, tested at voltages corresponding to a current density of 10 mA cm^{-2}. The bilayer capacity (C_{dl}) was used to measure the electrocatalytic surface active area of the catalyst. The CV curves of the catalysts were tested in 1 M KOH solution at different sweep rates (20, 40, 60, 80, 100 mV s^{-1}) in the potential range of 0.97-1.07 V， and C_{dl} calculated from equation (6).

$$C_{dl} = \frac{i}{v} \qquad (6)$$

where *i* is the current density and *v* is the sweep speed.

2.4 Assembly and testing of ZAB

The zinc-air battery (ZAB) was tested in an electrolyte solution containing 6 M KOH and 0.2 M $Zn(CH_3COO)_2$, zinc foil was used as the anode, and the air cathode was made from commercial carbon paper (P_2, Changsha Spring New Energy Technology Co., Ltd.) coated with catalysts (CoFeS/SNCNT or Pt/ C and RuO_2) ink (loading capacity is 1 mg cm^{-2}). All tests were carried out in CHI 760E. The specific capacity was calculated and normalized by using the amount of consumed Zn during discharge.

The Flexible ZAB consist of a 1 mm zinc plate as the anode, gel polymer as the electrolyte, and commercial carbon paper that was loaded with CoFeS/SNCNT as an air cathode. The gel electrolyte was prepared by the following steps: 3 g polyvinyl alcohol (PVA) was dissolved in 30ml water, magnetically stirred at 90℃ for 2 h, and then 3 mL 18 M KOH + 0.2 M $Zn(Ac)_2$ solution was added. After 1 h, a hot light yellow viscous

solution was obtained, which was immediately spread on a watch glass to form a 1-2 mm thick gel film, and freeze-dried for 12 h for later use.

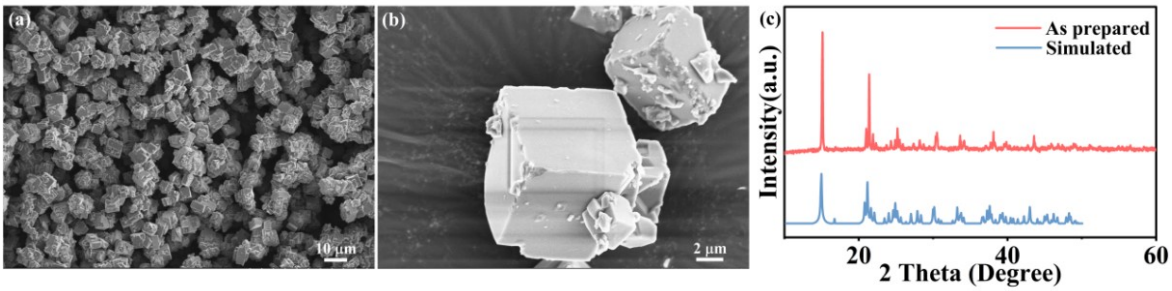

Fig. S1. (a, b) SEM images and (c) XRD spectra of Co-FF.

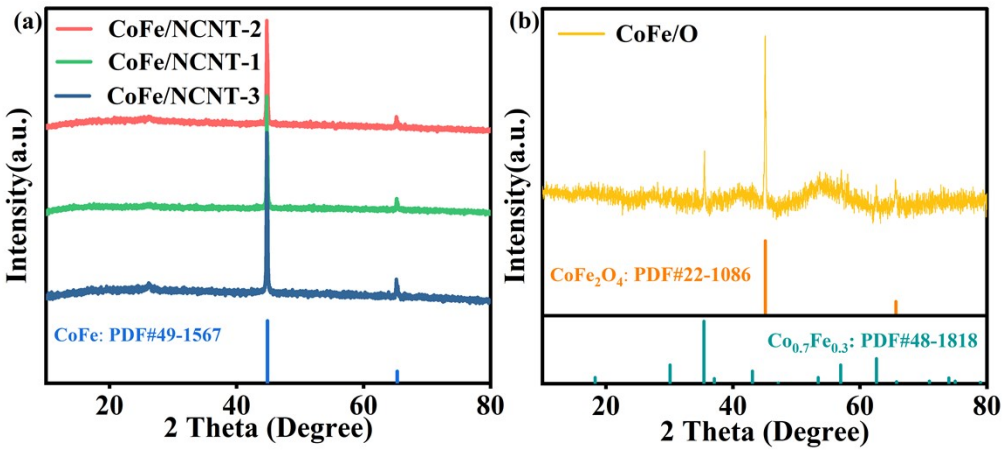

Fig. S2. XRD spectra of (a) CoFe/NCNT-1, CoFe/NCNT-2, CoFe/NCNT-3, and (b) CoFe/O.

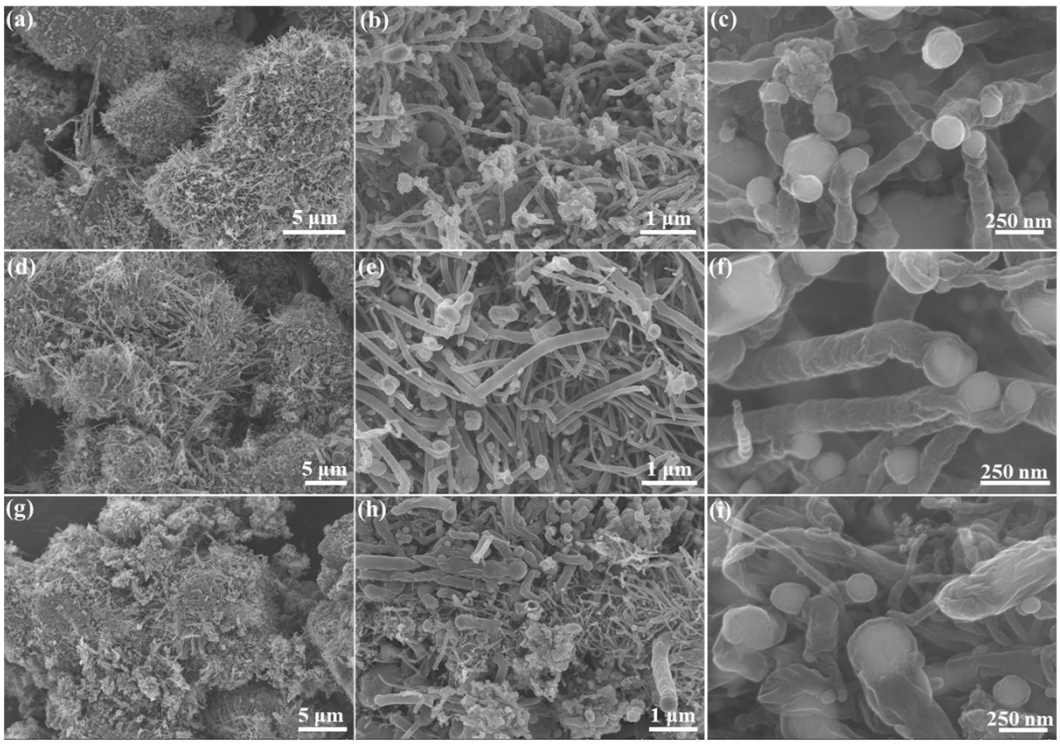

Fig. S3. SEM images of (a-c) CoFe/NCNT-1, (d-f) CoFe/NCNT-2 and (g-i) CoFe/NCNT-3.

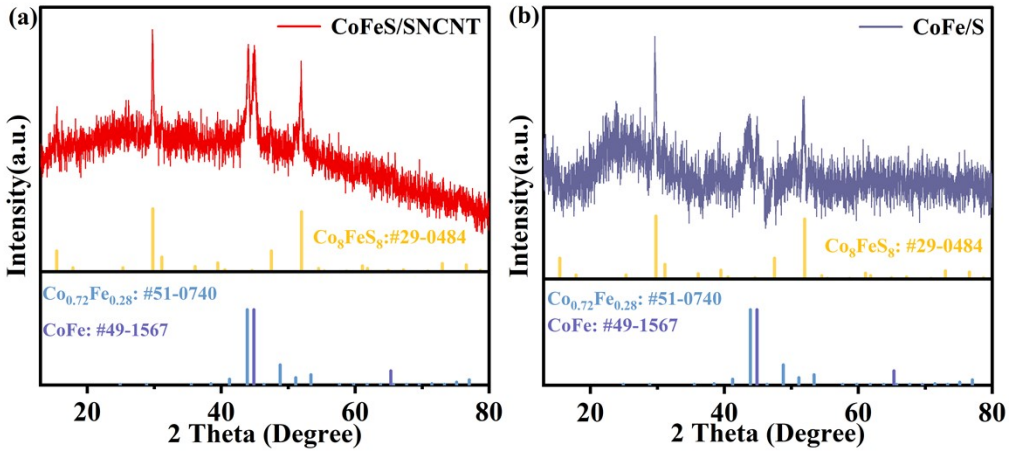

Fig. S4. XRD spectrum of (a) CoFeS/SNCNT and (b) CoFe/S.

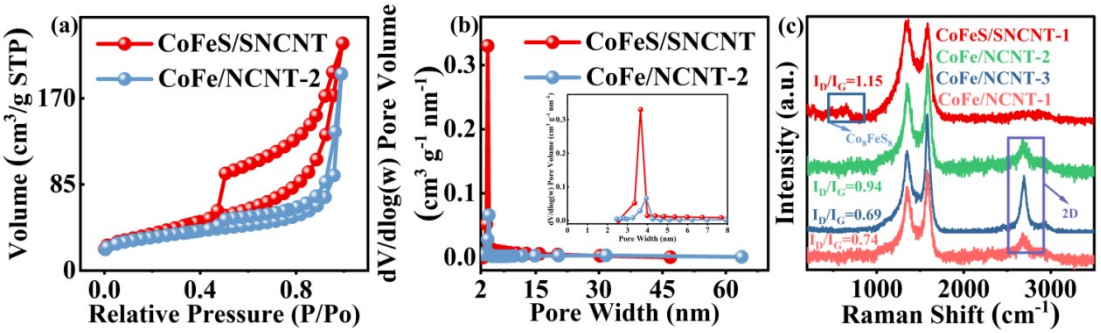

Fig. S5. (a) Adsorption-desorption isotherms and (b) BJH pore size distribution curves of CoFeS/SNCNT and CoFe/NCNT-2 (inset: enlarge image). (c) Raman spectra of the samples.

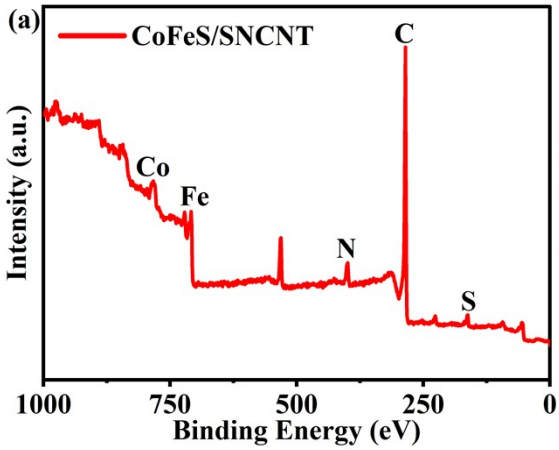

Fig. S6. XPS survey spectrum of CoFeS/SNCNT.

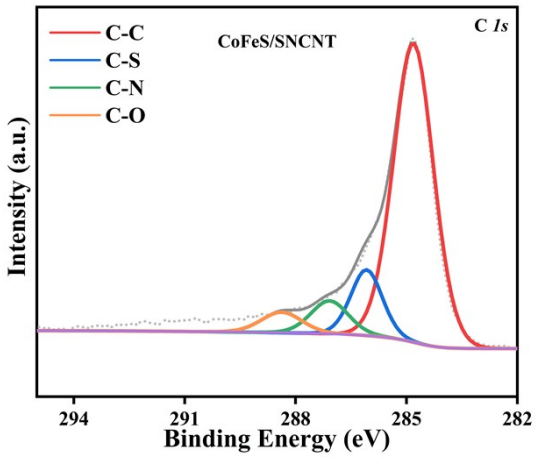

Fig. S7. High-resolution XPS spectrum of C 1s for CoFeS/SNCNT.

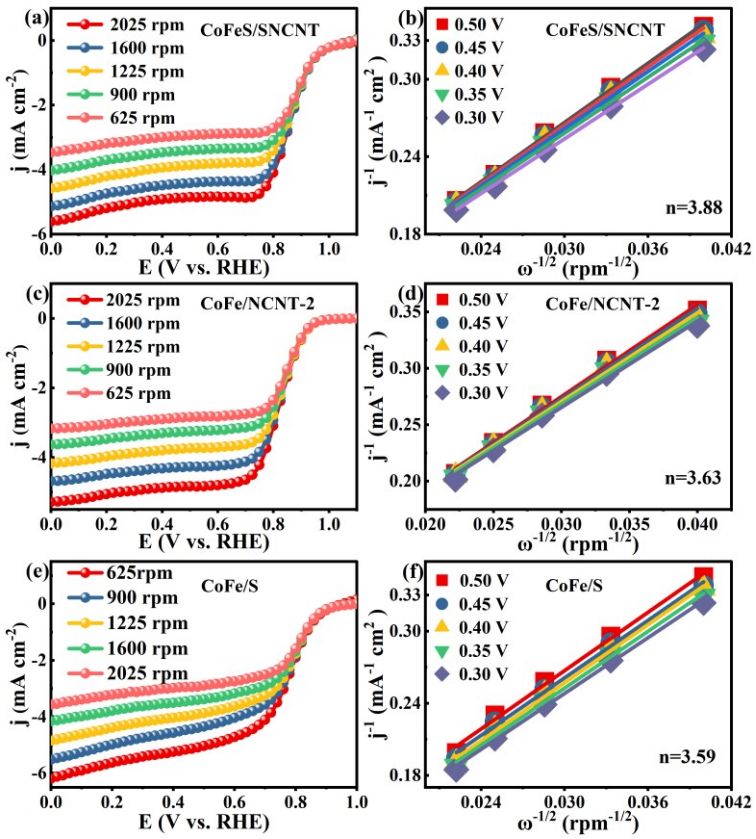

Fig. S8. LSV curves at different rotation rates and corresponding K-L plots at different potentials for (a, b) CoFeS/SNCNT, (c, d) CoFe/NCNT-2 and (e, f) CoFe/S.

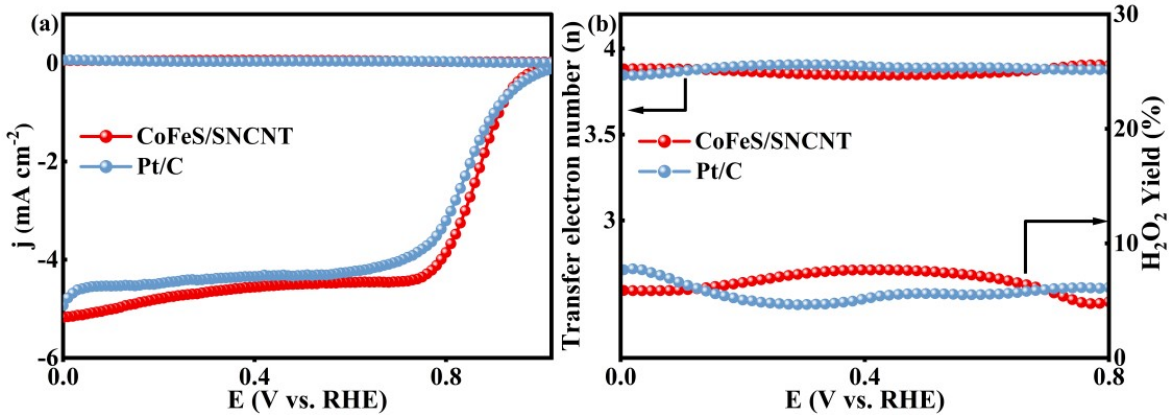

Fig. S9. (a) ORR polarization curves measured in the rotating ring-disk experiment, and (b) the calculated H_2O_2 yield and transfer electron number for CoFeS/SNCNT and Pt/C.

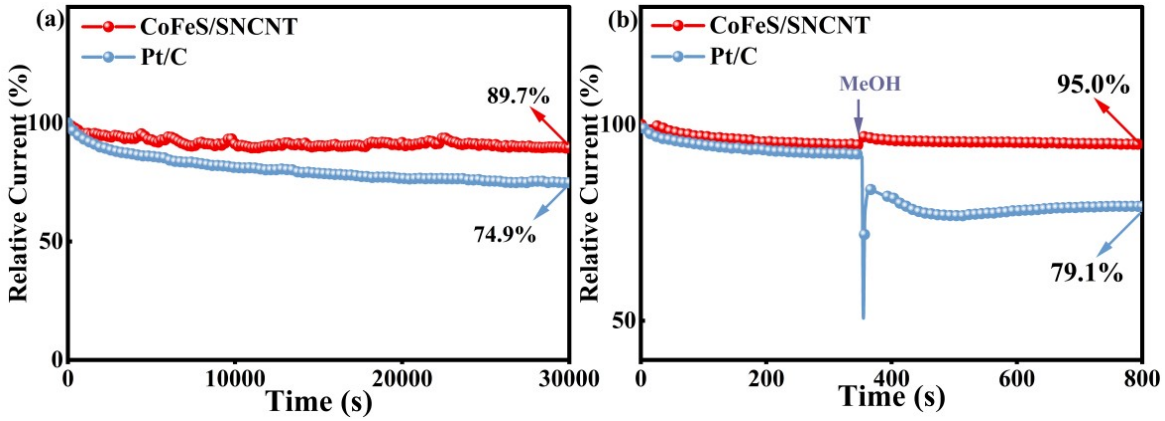

Fig. S10. (a) *I*-t curves and (b) methanol tolerance tests for CoFeS/SNCNT and Pt/C.

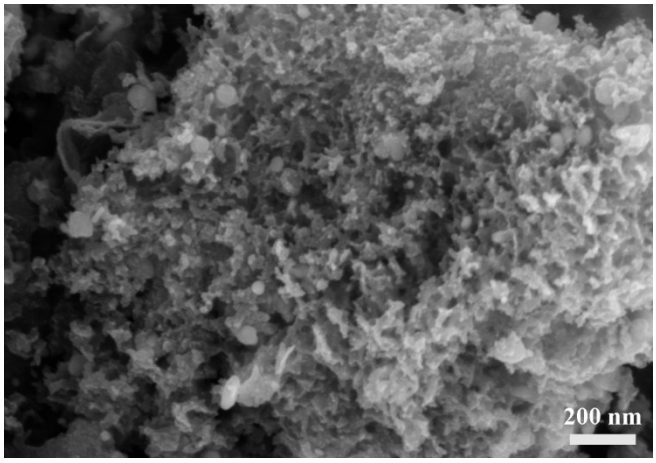

Fig. S11. SEM image of the CoFeS/SNCNT after ORR *I*-t test.

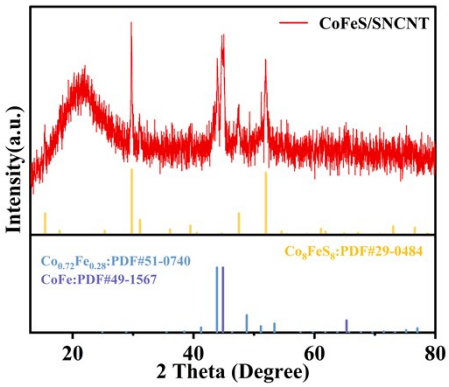

Fig. S12. XRD spectrum of CoFeS/SNCNT after ORR *I*-t test.

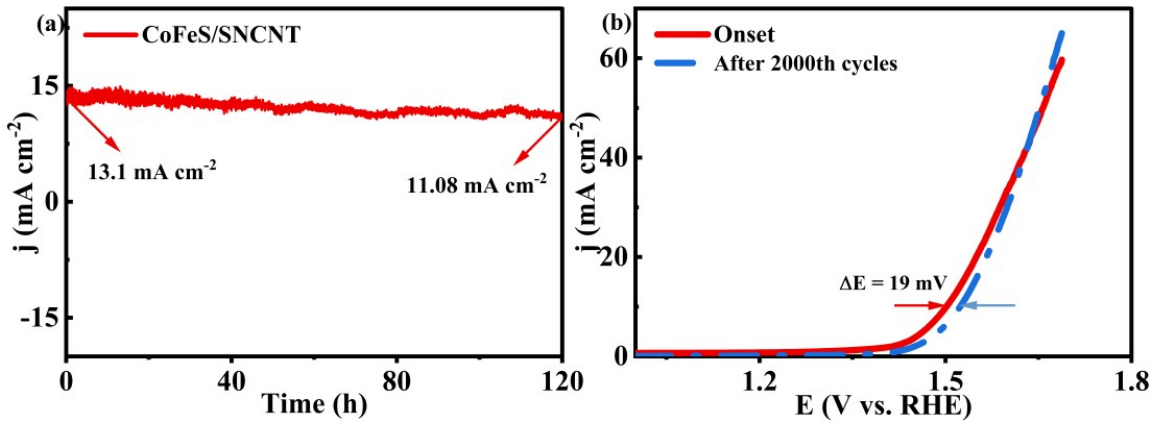

Fig. S13. (a) *I*-t curve and (b) ADT curves of CoFeS/SNCNT.

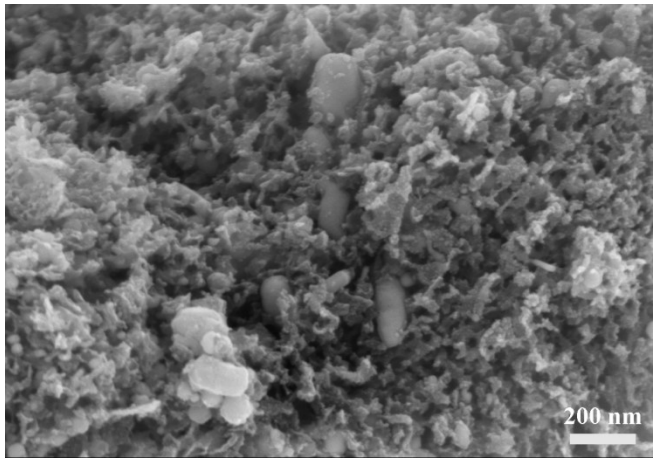

Fig. S14. SEM image of the CoFeS/SNCNT after OER *I*-t test.

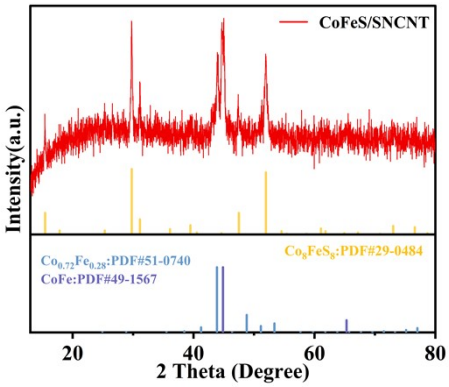

Fig. S15. XRD spectrum of CoFeS/SNCNT after OER *I*-t test.

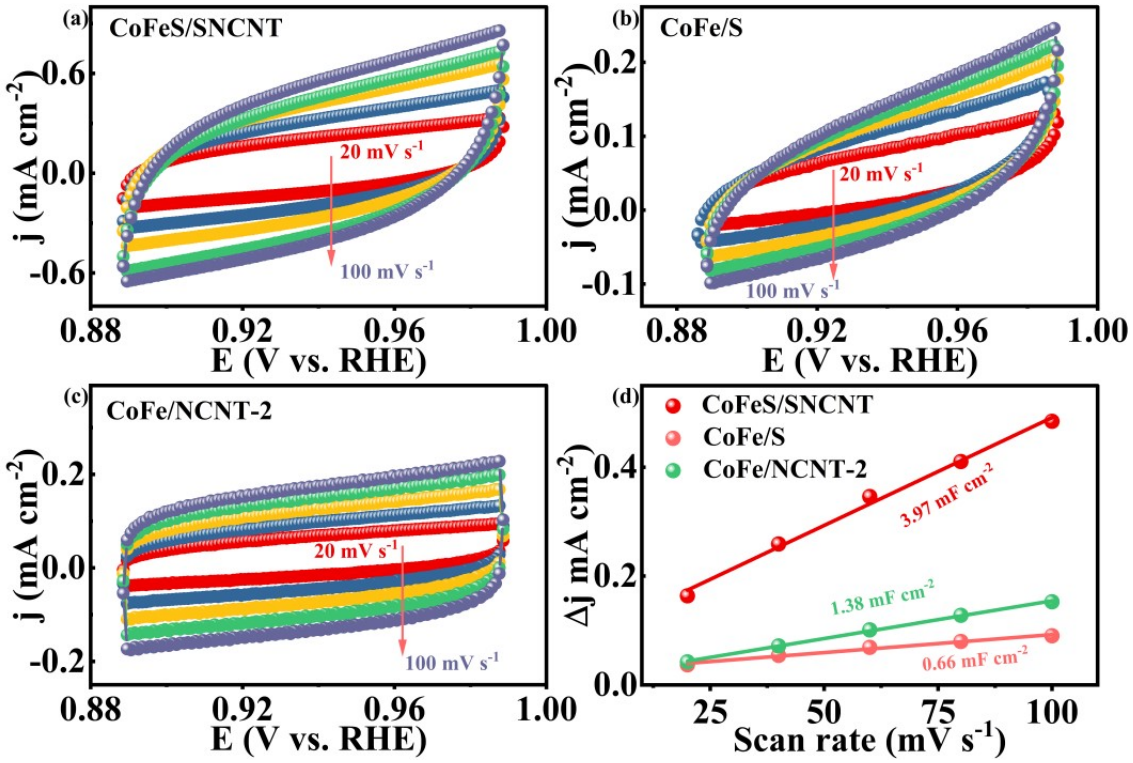

Fig. S16. CV curves of (a) CoFeS/SNCNT, (b) CoFe/S and (c) CoFe/NCT-2 with increasing scanning rate. (d) Calculated C_{dl} of the samples in the non-faraday interval.

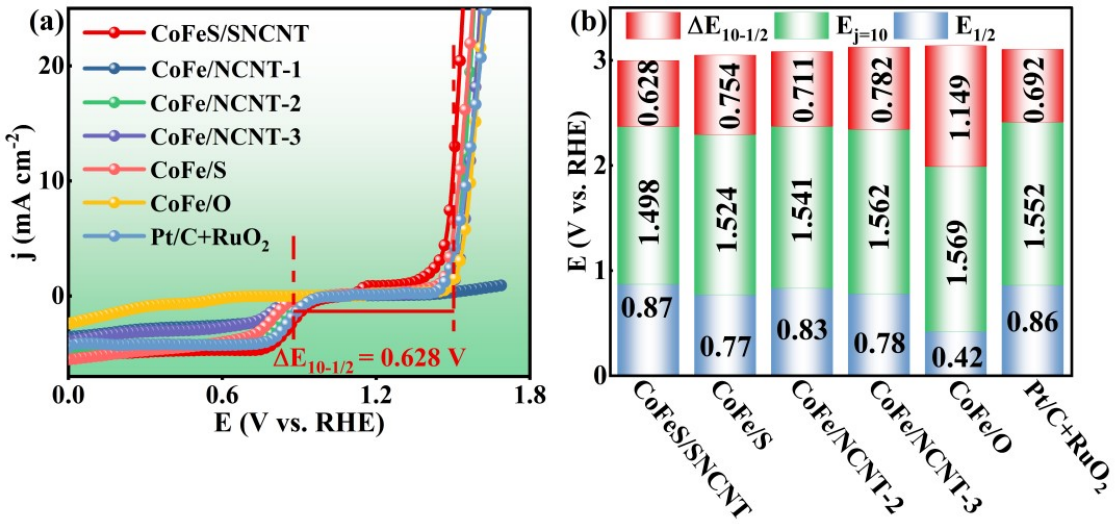

Fig. S17. (a) Polarization curves of ORR and OER and (b) histogram of ΔE, $E_{1/2}$ and $E_{j=10}$ for the samples.

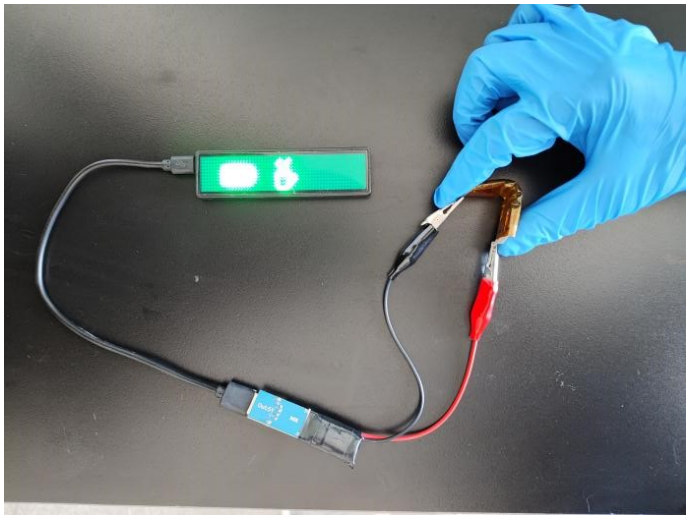

Fig. S18. Photograph of a LED device driven by the flexible ZAB@CoFe.

Table S1 Results of EDS spectrum of CoFeS/SNCNT.

Element	Atomic (%)	Mass (%)
C	88.1	68.8
N	3.1	2.8
S	2.5	5.2
Fe	5.1	18.4
Co	1.2	4.8

Table S2 Results of quantitative analysis of elements in CoFeS/SNCNT.

Elements	EA (wt%)	ICP (wt%)
C	26.74	——
N	3.24	——
S	11.04	——
Co	——	24.80
Fe	——	22.90

Table S3 Summary of the catalytic activities of the reported transition metal sulfide carbon-based electrocatalysts.

Electroatalysts	$E_{1/2}$ (V vs. RHE)	$E_{j=10}$ (V vs. RHE)	$\Delta E_{10-1/2}$ (V vs. RHE)	References
CoFeS/SNCNT	0.87	1.50	0.63	This work
NSC/Co_9S_8-200	0.83	1.63	0.8	[1]
CoFe/S-N-C	0.86	1.59	0.73	[2]
Co_9S_8@N, S–C	0.88	1.53	0.65	[3]
CoS_x/NCNTs/Ni-2	0.79	1.54	0.75	[4]
CoFe/SN-C	0.84	1.5	0.66	[5]
(Fe,Co)SPPc-900-sp	0.83	1.58	0.75	[6]
$Fe_1Co_1S_x$@NSPC	0.82	1.62	0.80	[7]
Co–Fe–S@NSRPC	0.80	1.6	0.80	[8]
Co-Ni-S@NSPC	0.82	1.70	0.88	[9]

References

1. Q. Zheng, Y. Xiong, K. Tang, M. Wu, H. Hu, T. Zhou, Y. Wu, Z. Cao, J. Sun, X. Yu and C. Wu, Modulation of pore-size in N, S-codoped carbon/Co_9S_8 hybrid for a stronger O_2 affinity toward rechargable zinc-air battery, *Nano Energy*, 2022, **92**, 106750.
2. G. Li, Y. Tang, T. Fu, Y. Xiang, Z. Xiong, Y. Si, C. Guo and Z. Jiang, S, N co-doped carbon nanotubes coupled with CoFe nanoparticles as an efficient bifunctional ORR/OER electrocatalyst for rechargeable Zn-air batteries, *Chem. Eng. J.,* 2022, **429**, 132174.
3. D. Lyu, S. Yao, A. Ali, Z. Q. Tian, P. Tsiakaras, P. K. Shen, N, S Codoped Carbon Matrix-Encapsulated Co_9S_8 Nanoparticles as a Highly Efficient and Durable Bifunctional Oxygen Redox Electrocatalyst for Rechargeable Zn–Air Batteries. *Adv. Energy Mater.,* 2021, **11**, 2101249.
4. L.-N. Lu, Y.-L. Luo, H.-J. Liu, Y.-X. Chen, K. Xiao and Z.-Q. Liu, Multivalent CoS_x coupled with N-doped CNTs/Ni as an advanced oxygen electrocatalyst for zinc-air batteries, *Chem. Eng. J.*, 2022, **427**, 132041.
5. C. Li, E. Zhou, Z. Yu, H. Liu and M. Xiong, Tailor-made open porous 2D CoFe/SN-carbon with slightly weakened adsorption strength of ORR/OER intermediates as remarkable electrocatalysts toward zinc-air batteries, *Appl. Catal. B Environ.* **2020**, 269, 118771.
6. L. Chen, L. L. Cui, Z. Wang, X. He, W. Zhang and T. Asefa, Co_8FeS_8/N,S-Doped Carbons Derived from Fe-Co/S-Bridged Polyphthalocyanine: Efficient Dual-Function Air-Electrode Catalysts for Rechargeable Zn-Air Batteries, *ACS Sustain. Chem. Eng.*, 2020, **8**, 13147-13158.
7. W. Fang, P. Dai, H. Hu, T. Jiang, H. Dong and M. Wu, $Fe_{0.96}S/Co_8FeS_8$ nanoparticles co-embedded in porous N, S codoped carbon with enhanced bifunctional electrocatalystic activities for all-solid-state Zn-air batteries, *Appl. Surf. Sci.,* 2020, **505**, 144212.
8. W. Fang, Z. Bai, X. Yu, W. Zhang and M. Wu, Pollen-derived porous carbon decorated with cobalt/iron sulfide hybrids as cathode catalysts for flexible all-solid-state rechargeable Zn–air batteries, *Nanoscale*, 2020, **12**, 11746-11758.

9. W. Fang, H. Hu, T. Jiang, G. Li and M. Wu, N- and S-doped porous carbon decorated with in-situ synthesized Co–Ni bimetallic sulfides particles: A cathode catalyst of rechargeable Zn-air batteries, *Carbon*, 2019, **146**, 476-485.